Strong Zero Modes from Geometric Chirality in Quasi-One-Dimensional Mott Insulators

Raul A. Santos[1] and Benjamin Béri[1,2]
[1]T.C.M. Group, Cavendish Laboratory, University of Cambridge, J.J. Thomson Avenue, Cambridge CB3 0HE, United Kingdom
[2]DAMTP, University of Cambridge, Wilberforce Road, Cambridge CB3 0WA, United Kingdom

(Received 2 June 2020; accepted 7 October 2020; published 9 November 2020)

Strong zero modes provide a paradigm for quantum many-body systems to encode local degrees of freedom that remain coherent far from the ground state. Example systems include $\mathbb{Z}_n$ chiral quantum clock models with strong zero modes related to $\mathbb{Z}_n$ parafermions. Here, we show how these models and their zero modes arise from geometric chirality in fermionic Mott insulators, focusing on $n = 3$ where the Mott insulators are three-leg ladders. We link such ladders to $\mathbb{Z}_3$ chiral clock models by combining bosonization with general symmetry considerations. We also introduce a concrete lattice model which we show to map to the $\mathbb{Z}_3$ chiral clock model, perturbed by the Uimin-Lai-Sutherland Hamiltonian arising via superexchange. We demonstrate the presence of strong zero modes in this perturbed model by showing that correlators of clock operators at the edge remain close to their initial value for times exponentially long in the system size, even at infinite temperature.

DOI: 10.1103/PhysRevLett.125.207201

Quantum many-body systems supporting local degrees of freedom that remain coherent for long times even away from the ground state may open up nonzero temperature, or even nonequilibrium, regimes for quantum information processing [1–17]. A key requirement for such coherence is the presence of degeneracies across the energy spectrum. "Strong zero modes" [3] provide a compelling mechanism for this (another route is by many-body localization [9–17]): these are objects that commute with the Hamiltonian (up to corrections exponentially decaying in system size), but they do not commute with a discrete symmetry, hence ensuring spectral degeneracies. When located at the system edge, they furthermore furnish the desired longtime-coherent local degrees of freedom [1–8].

One of the most intriguing paradigms where zero modes appear are quantum clock models with $\mathbb{Z}_{n\geq 3}$ symmetry [1–4]. The zero modes include $\mathbb{Z}_n$ parafermions, signifying a (nonlocal) relation to electronic systems proposed for beyond-Majorana schemes of topological quantum computation [1–4,18–33]. To support strong zero modes, the clock models require a chiral (i.e., reflection-symmetry breaking) deformation of their couplings [1–4,34–36]. While phase transitions in the chiral-quantum-clock-model universality class have seen realizations [37–41], the chiral quantum clock models themselves, and their strong zero modes, are yet to find their origin in an underlying microscopic system.

Here, we describe a paradigm for how chiral quantum clock models and their strong zero modes can arise in Mott insulators. While somewhat abstract in terms of clock models, chirality is a simple geometrical feature for particles hopping on a lattice [42], with examples such as chiral nanotubes, molecules, or crystals [43,44]. Our approach is centered on the combination of such geometric chirality with strong interactions.

We focus on the simplest case of $\mathbb{Z}_3$ symmetry and study spinless fermion systems such as the three-leg ladder in Fig. 1. We take two complementary approaches: (i) bosonization that captures generic features beyond a single microscopic model but which is only phenomenological in interactions, and (ii) strong-interaction perturbation theory for the system in Fig. 1. Using bosonization, we show how chiral-quantum-clock-model physics, including zero modes, can arise in the presence of certain symmetries

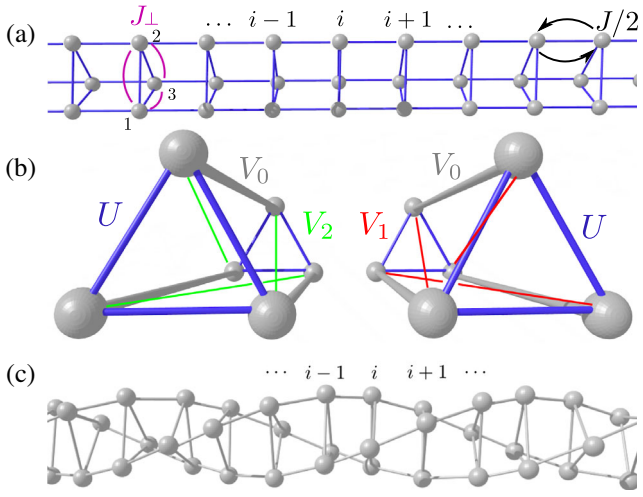

FIG. 1. Three-leg geometry for spinless fermions. (a) The hopping amplitudes J and $J_\perp$. (b) The interaction U between fermions at the same i and the interactions between neighboring sites V_0, V_1, and V_2. Geometric chirality [e.g., as in panel (c)] naturally leads to chiral interactions ($V_1 \neq V_2$).

(e.g., $\mathbb{Z}_3$ and time reversal) and sufficiently strong and chiral interactions. In our lattice system, we provide an explicit mapping to the chiral three-state clock model perturbed by terms arising via superexchange, and assess the presence of strong zero modes by computing dynamical correlators of clock operators at the edge using exact diagonalization.

Models and symmetries.—We set our terminology using the system in Fig. 1. Anticipating the clock-model mapping, we refer to the positions i along the legs as sites. The legs are of length ℓ and the sites are a_0 apart. The Hamiltonian is $H = H_0 + H_{\rm int}$ with

$$H_0 = -\frac{J}{2}\sum_{i,a} c^\dagger_{i,a} c_{i+1,a} + J_\perp \sum_{i,a} c^\dagger_{i,a} c_{i,a+1} + \text{H.c.},$$
$$H_{\rm int} = \sum_{i,a,b}\left(V_b n_{i,a} n_{i+1,a+b} + \frac{U}{2} n_{i,a} n_{i,b} \right). \quad (1)$$

Here, $c^\dagger_{i,a+3} = c^\dagger_{i,a}$ creates a fermion at site i and leg $a \in \{0,1,2\}$; $n_{i,a} = c^\dagger_{i,a} c_{i,a}$ is the corresponding number operator. We use real intraleg and interleg tunneling amplitudes J and $J_\perp$, respectively.

Geometric chirality is present if $V_1 \neq V_2$. We characterize this by introducing $V = \frac{1}{3}\sum_a V_a$ and

$$V' \sin\Phi = \frac{V_1 - V_2}{\sqrt{3}}, \qquad V' \cos\Phi = \frac{2V_0 - V_1 - V_2}{3}. \quad (2)$$

The system is invariant under the $\mathbb{Z}_3$ transformation $\mathcal{S}$ cyclically permuting the legs. Further symmetries include time-reversal $\mathcal{T}$ and, for the bulk physics (i.e., far from the boundaries), lattice translations along the legs. The generic systems we shall discuss are three-leg ladders beyond Eq. (1), but which still respect these symmetries [45]. We work at 1/3 filling, $\sum_{i,a} n_{i,a} a_0/\ell = 1$.

Low-energy processes.—We next prepare for bosonization by describing the low-energy bulk processes. By low energy, we mean processes near the Fermi points. Our bosonization thus starts with moderate interactions; however, its phenomenological scope is broader and includes strong interactions [46,47]. We first diagonalize the $\mathbb{Z}_3$ transformation using $f_{i,\alpha} = \sum_a v_{\alpha a} c_{i,a}$, where v is a 3×3 unitary matrix; this diagonalizes the single-particle Hamiltonian into three bands labeled by $\alpha \in \{1,2,3\}$ (Fig. 2 for our concrete model [48]). $\mathbb{Z}_3$ and time-reversal symmetries now act as $\mathcal{S} f_{j,\alpha} \mathcal{S}^{-1} = \omega^\alpha f_{j,\alpha}$ (where $\omega = e^{2\pi i/3}$), and $\mathcal{T} f_{j,1} \mathcal{T}^{-1} = f_{j,2}$, $\mathcal{T} f_{j,3} \mathcal{T}^{-1} = f_{j,3}$. At 1/3 filling, and for moderate band splitting [$J_\perp \lesssim J/3$ for Eq. (1)], there are six Fermi points $k_{F,\alpha}$. Working near $k_{F,\alpha}$, we can split $f_{j,\alpha}$ into left (L) and right (R) movers, $f_{j,\alpha}/\sqrt{a_0} = R_\alpha(x) e^{ik_{F,\alpha}x} + L_\alpha(x) e^{-ik_{F,\alpha}x}$, with $x = ja_0 \in [0,\ell]$. The symmetries (including crystal-momentum conservation) allow three classes of four-fermion processes: forward scattering, band-3 pairing, and "not-3" scattering. Forward scattering contributes to the quadratic part of the theory [46,47]. The band-3 pairings $O_{p1} = L_1^\dagger R_2^\dagger L_3 R_3$ and $O_{p2} = L_2^\dagger R_1^\dagger L_3 R_3$ describe the transfer between band-3 fermion pairs and fermions in bands 1, 2. Not-3 scattering $O_{\bar 3} = L_1^\dagger R_2^\dagger L_2 R_1$ does not involve band-3 fermions. These, and their Hermitian conjugates, are the lowest-order symmetry-allowed processes. They transfer R movers (and L movers) across different bands, but conserve their total number separately. To capture the phenomenology, we include the umklapp $O_u = L_1^\dagger L_2^\dagger L_3^\dagger R_1 R_2 R_3$, which is the lowest-order symmetry-allowed process scattering R and L movers into each other without interband transfer.

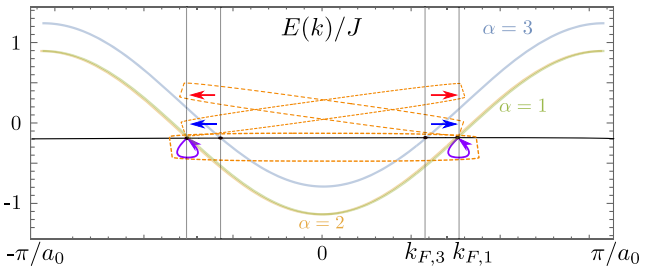

FIG. 2. The single-particle spectrum of H_0 in Eq. (1) for $J_\perp/J = 0.12$. Bands $\alpha = 1, 2$ remain degenerate for nonzero $J_\perp$ [48]. At 1/3 filling, momentum-conserving interband four-fermion processes combine pairs of two-fermion processes (arrows) between $k_{F,\alpha}$. The arrow colors indicate the bands involved (red, 3 and 1; blue, 3 and 2; purple, 1 and 2); the vertical offset is only for visualization. $\mathbb{Z}_3$ symmetry fixes the combinations to be those in the dashed boxes. Reversing all arrows gives the Hermitian conjugate processes.

Bosonization.—The complementary character of the $O_{a\neq u}$ and O_u processes translates to the separation into charge and neutral degrees of freedom. This becomes transparent in bosonization, an approach describing the corresponding density fluctuations [46,47]. We consider densities for charge $\tilde N_c = \sum_j N_j$ and neutral $\tilde N_1 = N_1 - N_2$, $\tilde N_2 = N_1 + N_2 - 2N_3$ combinations, where N_α is the particle number in band α. Note that $\mathcal{S} = \exp[(2\pi i/3)\tilde N_1]$, as implied by the transformation of f_α. We use conjugate pairs of fields θ_μ and φ_μ ($\mu = c, 1, 2$) whose only nonzero commutators are $[\theta_\mu(x), \varphi_\nu(y)] = i\delta_{\mu\nu}\Theta(x-y)$ with $\Theta(x)$ the Heaviside step function. The densities (relative to the Fermi sea) are $\rho_\mu = \sqrt{\beta_\mu/\pi}\partial_x\theta_\mu$ with $\beta_{c,1,2} = 3, 2, 6$. In terms of these fields, the band-α electron operators $\psi_{+\alpha} = R_\alpha$ and $\psi_{-\alpha} = L_\alpha$ are $\psi_{\eta\alpha} \propto (\kappa_\alpha/\sqrt{a_0}) \exp\{i\sqrt{\pi}[(\varphi_c + \eta\theta_c)/\sqrt{3} + \boldsymbol{d}_\alpha \cdot (\tilde{\boldsymbol{\varphi}} + \eta\tilde{\boldsymbol{\theta}})]\}$ where κ_α are Klein factors, $\tilde{\boldsymbol{\varphi}} = (\varphi_1, \varphi_2)$, $\tilde{\boldsymbol{\theta}} = (\theta_1, \theta_2)$, $\boldsymbol{d}_1 = (1/\sqrt{2}, 1/\sqrt{6})$, $\boldsymbol{d}_2 = (-1/\sqrt{2}, 1/\sqrt{6})$, $-\boldsymbol{d}_3 = \boldsymbol{d}_1 + \boldsymbol{d}_2$ [38,49,50]. At the boundaries ($x = 0, \ell$), zero charge current implies $\partial_x \varphi_c|_{x=0,\ell} = 0$; in the neutral sector we require only that boundary conditions respect $\mathcal{S}$ and $\mathcal{T}$.

The low-energy bulk Hamiltonian is $H_b = H_{\rm fw} + \int dx \mathcal{V}$. Here, $H_{\rm fw}$ encodes single-particle and forward-scattering terms. Although $H_{\rm fw}$ influences the phase diagram, for the essential features of the gapped regime we are interested in we can focus entirely on

$$\mathcal{V}(\theta_c, \theta_1, \varphi_2) = g_{\bar{3}} \cos\sqrt{8\pi}\theta_1 + g_2 \cos\sqrt{2\pi}\theta_1 \cos\sqrt{6\pi}\varphi_2 + g_1 \sin\sqrt{2\pi}\theta_1 \sin\sqrt{6\pi}\varphi_2 + g_u \cos\sqrt{12\pi}\theta_c \tag{3}$$

encoding the O_a processes. (We absorbed in $g_{1,2}$ the product $i\kappa_1\kappa_2$.) The following hold for the neutral-sector couplings $g_{1,2,\bar{3}}$, regardless of microscopic details: (i) interactions involving only the total density [such as the U term in Eq. (1)] conserve each band particle number and hence do not contribute to $g_{1,2}$; (ii) chirality enters via g_1 because spatial reflections take $O_{p1} \leftrightarrow O_{p2}$ and preserve $O_{\bar{3}}$, so $g_{2,\bar{3}}$ are invariant but g_1 changes sign.

The physics we are interested in is where $\mathcal{V}$ has deep minima confining $\theta_{c,1}$ and φ_2, a gapped regime that is expected to arise for sufficiently strong repulsive total-density interactions, as we shall confirm for our concrete model Eq. (1). Such strong microscopic interactions may place the problem beyond the scope of the weak-coupling renormalization group. One can, however, seek the chiral-clock-model phenomenology via a semiclassical analysis [46,47] of the field configurations that minimize $\mathcal{V}$. We start with the charge sector: the field θ_c is a constant locked to one of the minima of the umklapp cosine. The fluctuations $\rho_c \propto \partial_x \theta_c$ are thus absent; $1/3$ filling now means constant density of one particle per site.

The neutral sector works analogously. We focus on the chiral-clock-model phenomenology arising for $g_{\bar{3}} > 0$, a regime suggested by the contributions of strong repulsive total-density interactions. In the absence of chirality ($g_1 = 0$), a gap arises for large $|g_2| \gg g_{\bar{3}}$; in this case the fields $(\sqrt{2\pi}\theta_1, \sqrt{6\pi}\varphi_2)$ are locked to the configuration $\pi[n_x, n_x + 2n_y + \Theta(g_2)]$. For large $g_{\bar{3}} \gg |g_2|$, the system is gapless if $g_1 = 0$ and has central charge $c = 1$. These features for $|g_2| \gg g_{\bar{3}}$ and $g_{\bar{3}} \gg |g_2|$ are similar to those of the ordered and incommensurate phases of the nonchiral regimes of the clock model, respectively. Furthermore, the chiral coupling $g_1 \neq 0$ can open a gap for $g_{\bar{3}} \gg |g_2|$ (with locking configuration $\pi[n_x + \frac{1}{2}, n_x + 2n_y - \frac{1}{2}\,\mathrm{sgn}(g_1)]$), while for $|g_2| \gg g_{\bar{3}}$ it can close the gap (provided $|g_1| \approx |g_2|$), similarly to the effects of chiral deformations on the incommensurate and ordered phases of the clock model. The neutral part of $\mathcal{V}$ for $g_{\bar{3}} \gg |g_2|$ and $g_1 \neq 0$ is illustrated in Fig. 3.

The correspondence between the fermions $\psi_{\eta\alpha}$ and the fields θ_μ, φ_μ implies that the latter are periodic variables. In particular, $(\theta_c, \theta_1, \varphi_2) \sim (\theta_c, \theta_1, \varphi_2) + \sqrt{\pi}\boldsymbol{n} \cdot \boldsymbol{\Gamma}$ (together with a suitable shift of the conjugate pairs) where $\boldsymbol{n}$ is a vector of integers and the matrix $\boldsymbol{\Gamma}$ is

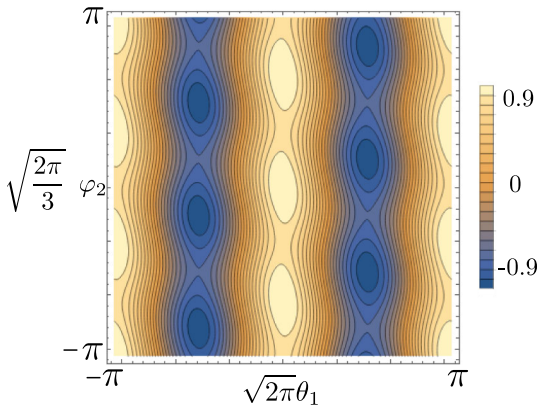

FIG. 3. The neutral part of $\mathcal{V}/|g_{\bar{3}}|$, for $g_1/g_{\bar{3}} = -0.15$, $g_2/g_{\bar{3}} = 0.1$ and $g_{\bar{3}} > 0$. Taking the compactification of the fields into account, there are six inequivalent minima (blue). For a given charge $\tilde{N}_c$ and $\mathbb{Z}_3$ label $\tilde{N}_1$ mod 3, the ground state corresponds to a superposition involving all six minima.

$$\boldsymbol{\Gamma} = \begin{pmatrix} \sqrt{3} & 0 & 0 \\ 0 & \sqrt{2} & 0 \\ 1/\sqrt{3} & -3/\sqrt{2} & 1/\sqrt{6} \end{pmatrix}.$$

Under this compactification, the six minima in Fig. 3, at a given θ_c, are inequivalent. Six inequivalent minima can also be arranged using a single θ_1 (and θ_c) but doubling the φ_2 interval. The operator $\exp(2\pi i\tilde{N}_2/6)$, which commutes with H_b, toggles between the six minima in the latter arrangement; since the values of $\tilde{N}_{c,1}$ specify $\exp(2\pi i\tilde{N}_2/6)$, for a given $\tilde{N}_{c,1}$ there is a single ground state corresponding to a superposition between the six minima. The presence of $\mathbb{Z}_3$ symmetry, however, guarantees the conservation only of $\tilde{N}_1$ mod 3; e.g., boundary terms (or corresponding neutral-sector boundary conditions) generically couple states with $\tilde{N}_1$ and $\tilde{N}_1 + 3$. For fixed particle number $\tilde{N}_c$, we are thus left with three towers of excitations, each labeled by its $\mathbb{Z}_3$ eigenvalue.

Zero modes.—A $\mathbb{Z}_3$ label in itself does not imply degeneracies in the spectrum. However, a threefold degeneracy arises if a zero-mode operator χ exists that commutes with the Hamiltonian while toggling the $\mathbb{Z}_3$ label. To obtain such zero modes, we consider the ground-state projections $\chi_{0,\ell}$ of neutral operators at the edge ($x = 0, \ell$), taking operators that change $\tilde{N}_1$ mod 3. Neutrality ensures maintaining a fixed particle number, while being at the edge means that $\chi_{0,\ell}$ create in (θ_1, φ_2) only boundary kinks, a feature compatible [18–21] with commutation with at least the ground state (or, more generally, subgap) sector of the Hamiltonian. As in parafermion systems, there are several choices for $\chi_{0,\ell}$ [21]. We choose $\chi_{0,\ell}$ as the ground-state projection of an operator $\mathcal{O}_\tau(x = 0, \ell)$ in the expansion of $f_1^\dagger f_2$, with $\mathcal{O}_\tau^\dagger \propto e^{i\frac{1}{3}\sqrt{12\pi}\theta_c} e^{i\sqrt{2\pi}\varphi_1} e^{i\frac{1}{3}\sqrt{6\pi}\theta_2}$. Hence, $\chi_{0,\ell}$ are local operators with $\chi_0\chi_\ell = \chi_\ell\chi_0$. They also satisfy $\chi_{0,\ell}\mathcal{S} = \omega\mathcal{S}\chi_{0,\ell}$, the requisite toggling of the $\mathbb{Z}_3$ label.

By introducing the nonlocal combination $\chi'_\ell = \mathcal{S}\chi_\ell$, we can also use a pair of mutual $\mathbb{Z}_3$ parafermions: $\chi_0\chi'_\ell = \omega\chi'_\ell\chi_0$. The phenomenology recovered here matches that of the chiral clock model [1–4], including the nonlocal nature of its parafermions. However, bosonization indicates the zero-mode character of $\chi^{(\prime)}_{0,\ell}$ only for subgap energies, which is sufficient only for their status as "weak" zero modes [4]. To study whether strong zero modes emerge, and for a concrete illustration of our bosonization phenomenology, we next turn to our microscopic model Eq. (1).

Strong-interaction perturbation theory.—We work deep in the Mott insulator regime $U \gg |J|$. We start with $J = J_\perp = V_a = 0$ in Eq. (1). This limit has a highly degenerate multiplet of lowest-energy states, each with one fermion per site. Turning on a small V_a and $J_\perp$ splits the low-energy states, without coupling to high-energy states with more than one fermion per site. In contrast, intraleg tunneling $H_J = -(J/2)\sum_{a,i} c^\dagger_{i,a}c_{i+1,a} + \text{H.c.}$ connects low- and high-energy states. To obtain the Hamiltonian governing the physics of low-energy states, we perform perturbation theory in J/U. The first nonzero correction is in second order in J/U, corresponding to a $\mathbb{Z}_3$ analog of superexchange. We find the effective Hamiltonian

$$H_{\text{eff}} = \sum_{j,a,b}\left(V_b n_{j,a}n_{j+1,a+b} + \frac{J^2}{2U}c^\dagger_{j,a}c_{j+1,a}c^\dagger_{j+1,b}c_{j,b}\right) + J_\perp\sum_{j,a}(c^\dagger_{j,a}c_{j,a+1} + \text{H.c.}), \tag{4}$$

valid for $U \gg |V_a|, |J|, |J_\perp|$.

Using the single occupation per site constraint $\sum_a n_{j,a} = 1$, we can rewrite H_{eff} in a form where the relation to the chiral clock model becomes manifest [51]. We map fermion bilinears to matrices $c^\dagger_{j,a}c_{j,b} \to M^{ab}_j$, with components $(M^{ab}_j)_{kl} = \delta_{ak}\delta_{bl}$ (omitting factors of identity away from site j). We find

$$H_{\text{eff}} = \sum_{j=1}^{N} J_\perp\sigma_j + \sum_{j=1}^{N-1}\frac{V'e^{i\Phi}}{2}\tau_j\tau^\dagger_{j+1} + \frac{J^2}{4U}P_{j,j+1} + \text{H.c.}, \tag{5}$$

where we have used Eq. (2) and $N = \ell/a_0$. Here, τ_j and σ_j are the clock variables

$$\tau_j = \begin{pmatrix} 1 & 0 & 0 \\ 0 & \omega & 0 \\ 0 & 0 & \omega^2 \end{pmatrix}, \qquad \sigma_j = \begin{pmatrix} 0 & 0 & 1 \\ 1 & 0 & 0 \\ 0 & 1 & 0 \end{pmatrix}, \tag{6}$$

while $P_{j,j+1}|a\rangle_j|b\rangle_{j+1} = |b\rangle_j|a\rangle_{j+1}$ is the swap operator between neighboring sites. For $J = 0$, Eq. (5) recovers the three-state quantum clock model. It is chiral for $\Phi \neq 0 \bmod \pi/3$ [1,4]. Equations (2) and (5) thus explicitly establish the link between geometric and clock-model chirality. For $J \neq 0$, the clock model is perturbed by the Uimin-Lai-Sutherland Hamiltonian [52–54], seen to arise here from superexchange.

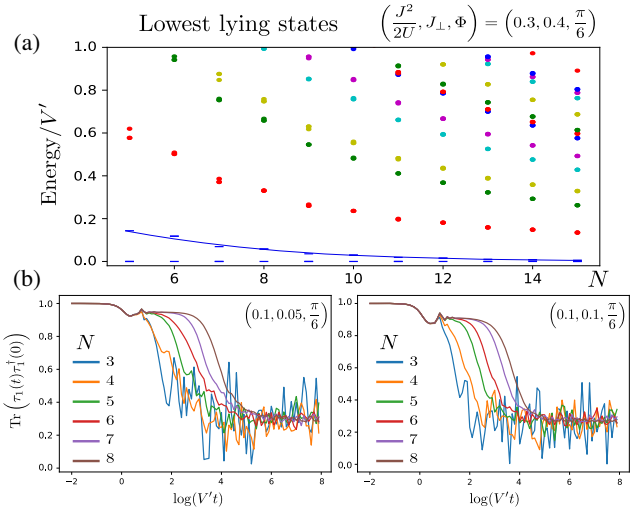

FIG. 4. (a) Low-lying energies of H_{eff}, measured from the ground state, for various system sizes N. The coloring changes for every three consecutive levels, repeating after the sixth color. The values of $J^2/2U$ and $J_\perp$ (shown at the top, with Φ) are measured in units of V'. The lowest excited states have energy (blue guide for the eye) consistent with ground-state-triplet splitting decaying exponentially with N. The excited-state-triplet splittings are barely visible on the scale of the figure. (b) The dynamical correlator $\text{Tr}[\tau_1(t)\tau_1^\dagger(0)]$. The persistence close to the initial value for times exponentially long in N indicates the presence of strong zero modes.

For $J = 0$, weak $J_\perp$, and Φ sufficiently away from 0 mod $\pi/3$, the system supports strong zero modes with the same properties as that of $\chi^{(\prime)}_{0,\ell}$ above [1]. Our next goal is to assess whether these strong zero modes survive the superexchange perturbation. We expect this for $|V'\sin(3\Phi)| \gg |J_\perp|, J^2/U$: here the combination of the spectral separation between various $J = J_\perp = 0$ domain-wall sectors and the scale separation between the chirality-induced intrasector splittings versus small $|J_\perp|, J^2/U$ might offer protection also against small nonzero J thanks to the restricted manner in which the swap operation acts on domain-wall states [51]. To assess the presence of strong zero modes, we first perform exact diagonalization to study the energy spectrum in this regime [Fig. 4(a)]. The existence of a zero mode that arranges the spectrum in $\mathbb{Z}_3$ triplets is manifest, both for the three lowest-lying states whose energy splitting decays consistently with an exponential in N, as well as for higher energies where the much smaller triplet splitting is almost invisible on the scale of the figure. Our findings are further corroborated by the $5 < N < 100$ excited-state spectrum in the single-domain-wall sector, where the $\mathbb{Z}_3$-triplet splittings decay exponentially with N to a value numerically indistinguishable from zero [51].

We next study dynamical consequences of these zero modes. Their edge-mode nature and exchange properties

with $\mathcal{S} = \prod_{j=1}^{N} \sigma_j$ suggest that they contribute significantly to τ_j at the boundary (in fact, $\tau_{1,N}$ are commuting zero modes for $J = J_\perp = 0$ [1,4], akin to $\chi_{0,\ell}$). We compute the infinite-temperature correlator [5,6]

$$\mathrm{Tr}[\tau_1(t)\tau_1^\dagger(0)] = 3^{-N}\sum_{k,j} |\langle k|\tau_1|j\rangle|^2 e^{i(E_k - E_j)t}, \qquad (7)$$

where E_j is the energy of the eigenstate $|j\rangle$. Time-independent contributions to the correlator come only from $|k\rangle$, $|j\rangle$ in degenerate triplets, provided $\langle k|\tau_1|j\rangle \neq 0$. (Diagonal matrix elements vanish due to $\tau_1\mathcal{S} = \omega\mathcal{S}\tau_1$.) For the signal to be appreciable, $\langle k|\tau_1|j\rangle \neq 0$ should hold for many degenerate triplets. In Fig. 4(b) we show the numerically evaluated correlator for two values of the parameters. (The behavior is similar for other values in the $|V' \sin(3\Phi)| \gg |J_\perp|, J^2/U$ regime, even for weakly disordered systems [51].) The results are consistent with the correlator remaining close to its initial value for times exponentially long in system size. Such behavior indicates exponentially decaying triplet splittings across the whole spectrum, and thus illustrates how strong zero modes lead to longtime coherence far from the ground state.

Conclusions.—We have shown how geometric chirality in a $\mathbb{Z}_3$- and $\mathcal{T}$-invariant Mott insulator can lead to chiral-quantum-clock-model physics, including strong zero modes. We illuminated this from two complementary perspectives: bosonization based on general symmetry considerations, and the analysis of the model Eq. (1) for strong interactions $U \gg |J|$. In our bosonization, after implementing the Mott-insulating regime by gapping out the charge degrees of freedom, we uncovered fingerprints of the ordered and incommensurate phases of the chiral quantum clock model, and established the presence of zero modes in the ordered phase. This suggests that chiral interactions provide a favorable setting for chiral-quantum-clock-model physics to arise in Mott insulators. Our model Eq. (1) gives concrete evidence for this: for $U \gg |J|$, we explicitly recover the chiral quantum clock model, perturbed by the Uimin-Lai-Sutherland Hamiltonian via superexchange. Our simulations suggest that the strong zero modes survive the superexchange perturbation, leading to the correlators of clock operators at the edge to persist near their initial value for times exponentially long in system size, even at infinite temperature. Interesting directions for future research include the study of the phase diagram and dynamics of our model with approaches that probe the thermodynamic limit. This will, in particular, illuminate where the zero modes we found fall in the refined "strong" versus "almost strong" classification of Refs. [5,6].

We acknowledge discussions with D. Gutman, K. Snizhko, F. Buccheri, and J. Park, and we thank P. Fendley for feedback on the manuscript. This work was supported by the ERC Starting Grant No. 678795 TopInSy.

[1] P. Fendley, J. Stat. Mech. (2012) P11020.
[2] P. Fendley, J. Phys. A **47**, 075001 (2014).
[3] P. Fendley, J. Phys. A **49**, 30LT01 (2016).
[4] J. Alicea and P. Fendley, Annu. Rev. Condens. Matter Phys. **7**, 119 (2016).
[5] J. Kemp, N. Y. Yao, C. R. Laumann, and P. Fendley, J. Stat. Mech. (2017) 063105.
[6] D. V. Else, P. Fendley, J. Kemp, and C. Nayak, Phys. Rev. X **7**, 041062 (2017).
[7] J. Kemp, N. Y. Yao, and C. R. Laumann, arXiv:1912.05546.
[8] D. J. Yates, A. G. Abanov, and A. Mitra, Phys. Rev. Lett. **124**, 206803 (2020).
[9] J. R. Wootton and J. K. Pachos, Phys. Rev. Lett. **107**, 030503 (2011).
[10] C. Stark, L. Pollet, A. Imamoğlu, and R. Renner, Phys. Rev. Lett. **107**, 030504 (2011).
[11] B. Bauer and C. Nayak, J. Stat. Mech. (2013) P09005.
[12] D. A. Huse, R. Nandkishore, V. Oganesyan, A. Pal, and S. L. Sondhi, Phys. Rev. B **88**, 014206 (2013).
[13] S. A. Parameswaran, A. C. Potter, and R. Vasseur, Ann. Phys. (Amsterdam) **529**, 1600302 (2017).
[14] F. Alet and N. Laflorencie, C. R. Phys. **19**, 498 (2018).
[15] S. A. Parameswaran and R. Vasseur, Rep. Prog. Phys. **81**, 082501 (2018).
[16] D. A. Abanin, E. Altman, I. Bloch, and M. Serbyn, Rev. Mod. Phys. **91**, 021001 (2019).
[17] T. B. Wahl and B. Béri, Phys. Rev. Research **2**, 033099 (2020).
[18] N. H. Lindner, E. Berg, G. Refael, and A. Stern, Phys. Rev. X **2**, 041002 (2012).
[19] M. Cheng, Phys. Rev. B **86**, 195126 (2012).
[20] D. J. Clarke, J. Alicea, and K. Shtengel, Nat. Commun. **4**, 1348 (2013).
[21] R. S. K. Mong, D. J. Clarke, J. Alicea, N. H. Lindner, P. Fendley, C. Nayak, Y. Oreg, A. Stern, E. Berg, K. Shtengel, and M. P. A. Fisher, Phys. Rev. X **4**, 011036 (2014).
[22] A. M. Tsvelik, Phys. Rev. Lett. **113**, 066401 (2014).
[23] J. Klinovaja and D. Loss, Phys. Rev. Lett. **112**, 246403 (2014).
[24] F. Zhang and C. L. Kane, Phys. Rev. Lett. **113**, 036401 (2014).
[25] C. P. Orth, R. P. Tiwari, T. Meng, and T. L. Schmidt, Phys. Rev. B **91**, 081406(R) (2015).
[26] A. Alexandradinata, N. Regnault, C. Fang, M. J. Gilbert, and B. A. Bernevig, Phys. Rev. B **94**, 125103 (2016).
[27] Y. Alavirad, D. Clarke, A. Nag, and J. D. Sau, Phys. Rev. Lett. **119**, 217701 (2017).
[28] A. Calzona, T. Meng, M. Sassetti, and T. L. Schmidt, Phys. Rev. B **98**, 201110(R) (2018).
[29] L. Mazza, F. Iemini, M. Dalmonte, and C. Mora, Phys. Rev. B **98**, 201109(R) (2018).
[30] A. Hutter and D. Loss, Phys. Rev. B **93**, 125105 (2016).
[31] J. Alicea and A. Stern, Phys. Scr. **T164**, 014006 (2015).
[32] A. Chew, D. F. Mross, and J. Alicea, Phys. Rev. B **98**, 085143 (2018).
[33] R. A. Santos, D. B. Gutman, and S. T. Carr, Phys. Rev. B **99**, 075129 (2019).
[34] A. S. Jermyn, R. S. K. Mong, J. Alicea, and P. Fendley, Phys. Rev. B **90**, 165106 (2014).

[35] Y. Zhuang, H. J. Changlani, N. M. Tubman, and T. L. Hughes, Phys. Rev. B **92**, 035154 (2015).
[36] N. Moran, D. Pellegrino, J. K. Slingerland, and G. Kells, Phys. Rev. B **95**, 235127 (2017).
[37] P. Fendley, K. Sengupta, and S. Sachdev, Phys. Rev. B **69**, 075106 (2004).
[38] P. Lecheminant and H. Nonne, Phys. Rev. B **85**, 195121 (2012).
[39] A. M. Tsvelik and A. B. Kuklov, New J. Phys. **14**, 115033 (2012).
[40] R. Samajdar, S. Choi, H. Pichler, M. D. Lukin, and S. Sachdev, Phys. Rev. A **98**, 023614 (2018).
[41] A. Keesling, A. Omran, H. Levine, H. Bernien, H. Pichler, S. Choi, R. Samajdar, S. Schwartz, P. Silvi, S. Sachdev *et al.*, Nature (London) **568**, 207 (2019).
[42] A. B. Buda, T. A. der Heyde, and K. Mislow, Angew. Chem. **31**, 989 (1992).
[43] R. Saito, G. Dresselhaus, and M. S. Dresselhaus, *Physical Properties of Carbon Nanotubes* (World Scientific, Singapore, 1998).
[44] G. D. Fasman, *Circular Dichroism and the Conformational Analysis of Biomolecules* (Springer, New York, 2013).
[45] The model is also invariant under reflection along the legs combined with exchanging two of the legs; this symmetry can be used instead of time reversal in our considerations.
[46] T. Giamarchi, *Quantum Physics in One Dimension* (Clarendon Press, Oxford, 2003).
[47] A. Gogolin, A. Nersesyan, and A. Tsvelik, *Bosonization and Strongly Correlated Systems* (Cambridge University Press, Cambridge, England, 2004).
[48] The model's single-particle Hamiltonian H_0 has a reflection symmetry which leads to $k_{F,1} = k_{F,2}$; however, this is not a generic feature. All the processes we consider survive in the more general $\mathbb{Z}_3$- and time-reversal-invariant case with split $k_{F,1}$ and $k_{F,2}$.
[49] J. C. Y. Teo and C. L. Kane, Phys. Rev. B **89**, 085101 (2014).
[50] M. Fabrizio and A. O. Gogolin, Phys. Rev. B **51**, 17827 (1995).
[51] See Supplemental Material at http://link.aps.org/supplemental/10.1103/PhysRevLett.125.207201 for details on the correspondence between Eqs. (4) and (5), our domain-wall considerations, and for additional numerical results.
[52] G. V. Uimin, JETP Lett. **12**, 225 (1970), http://www.jetpletters.ac.ru/cgi-bin/articles/download.cgi/1730/article_26296.pdf.
[53] C. K. Lai, J. Math. Phys. (N.Y.) **15**, 1675 (1974).
[54] B. Sutherland, Phys. Rev. B **12**, 3795 (1975).